Enhancement of light extraction efficiency of remote phosphor white light-emitting diode using a hemiellipsoidal antireflection subwavelength structure polyethylene terephthalate film

YUNG-FANG CHOU[a], CHI-FENG CHEN[a,*], SHANG-PING YING[b], YUN-YING YEH[a]
[a]*Department of Mechanical Engineering, National Central University, Taoyuan City 32001, Taiwan (R.O.C.)*
[b]*Department of Optoelectronic System Engineering, Minghsin University of Science & Technology, HsinChu 30401, Taiwan (R.O.C.)*

This study enhanced the light extraction efficiency (LEE) of a remote phosphor white LED by using a hemiellipsoidal antireflection subwavelength structure (ASS) polyethylene terephthalate (PET) film. The PET film was fabricated and combined with a hemiellipsoidal ASS on the surface of a remote phosphor white LED through a UV-curing adhesive process. The improvements in the LEE of the remote phosphor white LED with an ASS PET film are 11.76% and 23.26% compared with the remote phosphor white LED and conventional phosphor-converted white LED.

(Received May 29, 2016; accepted June 7, 2017)

Keywords: FDTD, Light extraction efficiency, Antireflection subwavelength structure, Remote phosphor white LED

1. Introduction

Recently, white LEDs based on phosphor conversion have accounted for a considerable proportion of the LED market [1]. To meet the requirements of sustainable development, continual enhancement of LED luminous efficiency is crucial. A remote phosphor package is an efficient method for enhancing luminous efficiency [2]. But inside remote phosphor white LEDs, some rays still generate Fresnel Reflection effect because of the difference in the refractive index of the fluorescent encapsulation layer and the air. The rays cannot be emitted to the air from the fluorescent encapsulation layer. When the incidence angle increases, the reflection effect becomes increasingly stronger. When the incident angle exceeds a critical angle, the total reflection effect of light occurs. The rays become confined within the LEDs, thereby reducing the optical efficiency of the remote phosphor white LEDs.

In order to enhance light extraction efficiency (LEE) of the LEDs many attempts for example like surface roughening by chemical etching [3,4], patterned sapphire substrates (PSSs) [5,6], placing photonic crystals (PCs) on top [7-10] and are made to suppress the Fresnel Reflection and TIR. But these methods are critical in improving the LEE of blue rays emitted from the GaN wafer to the transparent encapsulation layer. Regarding research on improving the efficiency of blue and yellow rays passing through the interface between the fluorescent encapsulation layer and air, few studies have adopted the method of modifying the shape of the white LED phosphor encapsulation layer geometry (encapsulant dome) to ensure that the rays emitted from the LED chip can progress nearly perpendicular to the fluorescent encapsulation layer–air interface [11,12].

In this study, we design and fabricate periodic antireflection subwavelength structure (ASS) upon a flexible PET film. The structure is designed by the finite difference time domain (FDTD) method and fabricated by roll-to-roll micro-replication process. Then we combine the PET film with ASS on the surface of remote phosphor white LEDs through UV curing. We demonstrate that remote phosphor white LEDs with ASS PET film have significantly improved LEE because both the total internal reflection and the Fresnel Reflection are reduced. Fig. 1 illustrates the schematic cross-sectional views of a (a) conventional phosphor-converted white LED (Cpc-LED), (b) remote phosphor white LED (Rpc-LED), and (c) remote phosphor white LED with an ASS PET film (ASS-Rpc-LED). Here, the Cpc-LED has a phosphor-in-cup structure and the ASS is hemiellipsoidal.

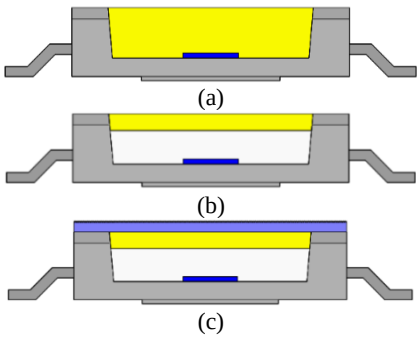

Fig. 1. Schematic cross-sectional views of the (a) Cpc-LED, (b) Rpc-LED, and (c) ASS-Rpc-LED

2. Simulation

In order to prove that periodic hemiellipsoidal subwavelength structures can improve LEE of the PET film, we used the three-dimensional FDTD [13,14] methods to quantitatively investigate the LEE enhancement. The PET film thickness was 188 μm. To reduce the time of the calculation, we took the simulation domain to be 10 μm × 10 μm (length × width), and the refractive indices of vacuum and PET were set to 1 and 1.57, respectively. The ASS comprised a plurality of hemiellipsoids in a hexagonal close-packed (HCP) arrangement on top of the PET film. The hemiellipsoidal structures having intervals and heights ranging from 100 to 600 nm, and the increment was 50 nm. The interval was twice the diameter. Perfect matched layers (PML) boundary conditions were applied on the boundaries in order to avoid unnecessary reflection of light at the boundaries of domain as well as reduce the domain size. The bottom surface was set to a perfectly reflecting surface. The detection monitor was positioned in the upper part of the analysis area. A single dipole source with a wavelength range of 400–700 nm was chosen and positioned in the center of x-y plane and also in the center of the PET film in the vertical direction. Fig. 2 illustrates the schematics of the FDTD simulation model, respectively.

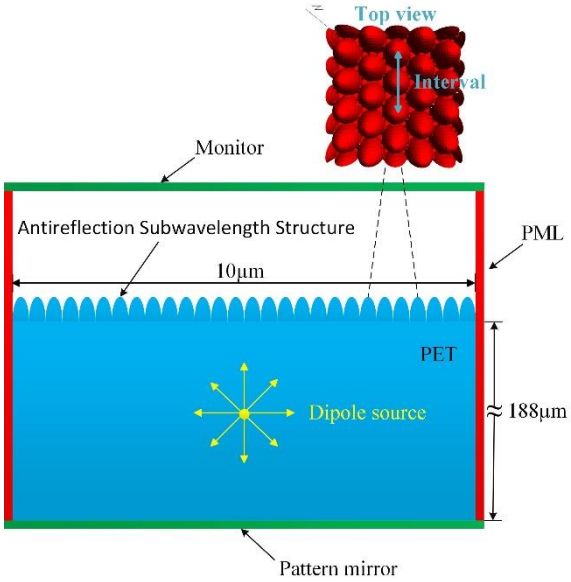

Fig. 2. Schematics of the three-dimensional FDTD simulation model (not to scale)

Because the far-field intensity distributions are proportional to LEE. The LEE for PET films was calculated by taking the ratio of the total power extracted from the PET film, which was obtained by integrating the far-field power density over all solid angle, with the total power radiated the dipole as measured the monitor. The LEE enhancement factor *F* is defined as

$$F = \frac{LEE_{with\ ASS} - LEE_{without\ ASS}}{LEE_{without\ ASS}} \times 100\% \quad (1)$$

Where $LEE_{with\ ASS}$ is the LEE of the PET film with ASS and $LEE_{without\ ASS}$ is the LEE of the PET film without ASS. We simulated LEE of the structures having different intervals and heights to optimize the efficiencies due to different dimensions of the hemiellipsoidal structure on the PET film. Fig. 3 shows the contour diagram for the light extraction efficiency enhancement factor F of the hemiellipsoidal structures having different intervals and heights. The contour diagram reveals two features: (i) The LEE enhancement factor F varied significantly with respect to the interval and height of different hemiellipsoidal structure. (ii) The structures providing higher enhancements were generally positioned in the left-hand regions of the contour diagram, indicating that a dense structure is preferred for light extraction. The hemiellipsoidal structure having an interval of 350 nm and a height of 300 nm provides the highest light extraction enhancement factor F of 13.30% in our simulation region. It can be inferred that PET film with ASS has a higher LEE due to both the total internal reflection and the Fresnel Reflection are reduced.

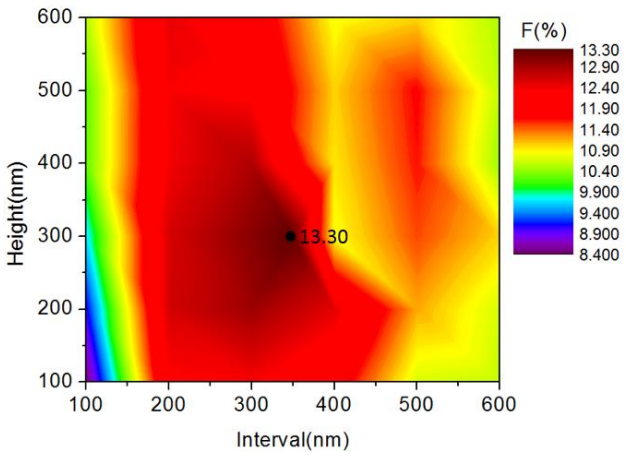

Fig. 3. Contour diagram for the LEE enhancement factor F of the hemiellipsoidal structure

The comparison for the far-field intensity distributions of the PET films without and with ASS was presented in Figs. 4(a) and 4(b). The diameter and interval of ASS on the PET film used in this research were 175 nm and 350 nm, and the height of the structure was 300 nm. From the simulation results, a PET film with ASS has a higher far-field intensity distributions. The far-field intensity distributions for PET films without ASS, as expected, exhibited Lambertian distribution with only angular(θ) dependent, while the symmetrically azimuthal(φ) distribution, as shown in Fig. 4(a). Note that the far-field intensity distributions for 2-D hexagonal close-packed hemiellipsoid arrays PET film exhibits both angular and azimuthal dependent, as shown in Fig. 4(b).

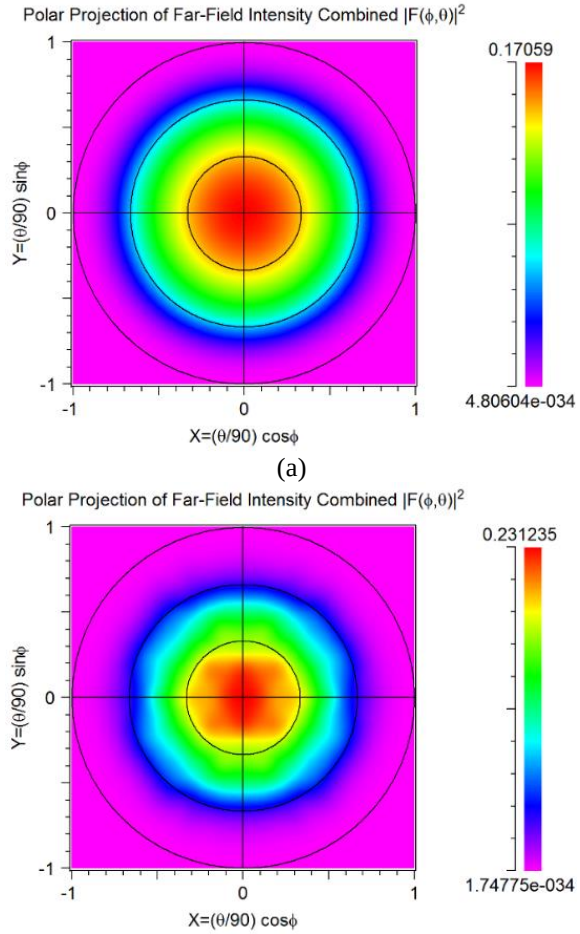

Fig. 4. Far-field intensity distributions of a PET film (a) without and (b) with ASS

3. Experiment

Micro-replication [15-17] was used to duplicate ASS on a flexible PET substrate through a UV-forming process. Micro-replication was combined with the originated structure fabrication realized through interference lithography [18,19], Ni mold electroplation [20], and replication by using UV imprinting [21, 22] into plastics. A Ni mold used for transferring the photoresist structure template fabricated through interference lithography was manufactured using micro-electroplating. With a Ni mold, the ASS was duplicated through UV imprinting based on a roll-to-roll technology. After UV curing, a flexible PET film with ASS can be peeled off from the Ni mold. Fig. 5 shows the schematic illustration of roll-to-roll micro-replication process. Figs. 6(a) and 6(b) show the SEM image of the prototype. The ASS was successfully duplicated through micro-replication.

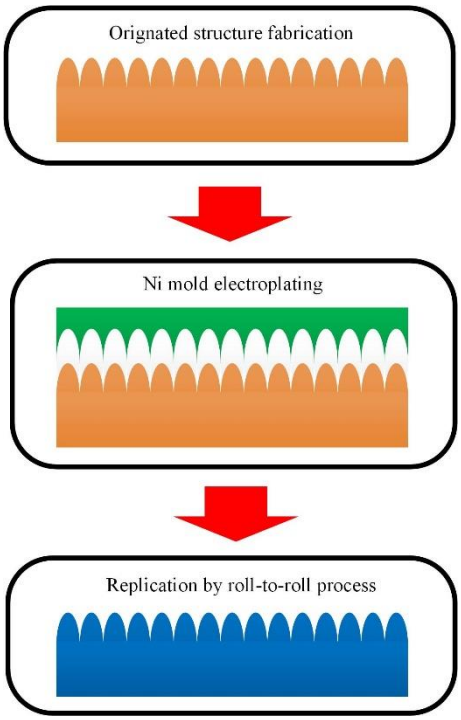

Fig. 5. Schematic illustration of roll-to-roll micro- replication process

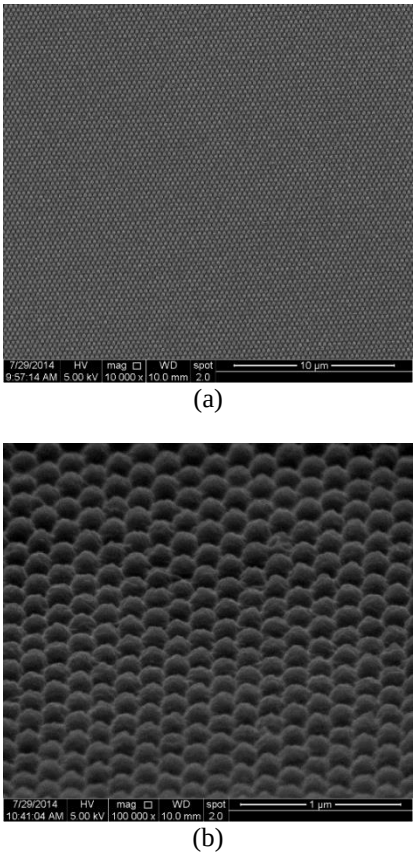

Fig. 6. (a)10 kx and (b)100 kx and tiled 75° SEM image of the hemiellipsoidal ASS array

To assess the effects of the remote phosphor package and ASS on the LEE of a white LED, Cpc-LED, Rpc-LED, and ASS-Rpc-LED samples were prepared. Achieving an objective comparison required using the same blue LED chip, reflector cup, and phosphor. To fabricate the ASS-Rpc-LED, the completed Rpc-LED was used and the fabricated PET film was cut to fit the shape of Rpc-LED and combined with ASS on the surface through UV curing. Figs. 7(a) and 7(b) show Rpc-LED and light test of ASS-Rpc-LED. To avoid the influence of wafer temperature variation on luminous efficiency and the radiation spectrum, an Instrument Systems CAS 140CT CCD array spectrometer and integrating sphere with a 30-cm diameter were used.

(a)

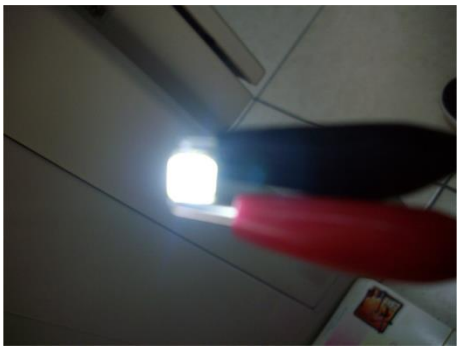

(b)

Fig. 7. (a) Rpc-LED and (b) Light test of ASS-Rpc-LED under 350mA

4. Results and discussion

The measurement results of the test LEDs for the variations in the output luminous flux and luminous efficiency as the function of injection current are shown in Figs. 8(a) and 8(b), respectively. As shown in Fig. 8(a), for three cases, the output luminous fluxes of the Cpc-LED, Rpc-LED, and ASS-Rpc-LED are 76.62, 84.46, and 94.47 lm, respectively. The calculation results showed that the improvements in the output luminous fluxes of the ASS-Rpc-LED are approximately 11.85% [(94.47 - 84.46) / 84.46 × 100% = 11.85%] and 23.30% [(94.47 – 76.62) / 76.62 × 100% = 23.30%] compared with those of the Rpc-LED and Cpc-LED, respectively. As shown in Fig. 8(b), for three cases, the luminous efficiencies of the Cpc-LED, Rpc-LED, and ASS-Rpc-LED are 67.41, 74.35, and 83.09 lm/W, respectively. The improvements in the luminous efficiencies of the ASS-Rpc-LED are 11.76% [(83.09 – 74.35) / 74.35 × 100% = 11.76%] and 23.26% [(83.09 – 67.41) / 67.41 × 100% = 23.26%] compared with those of the Rpc-LED and Cpc-LED, respectively.

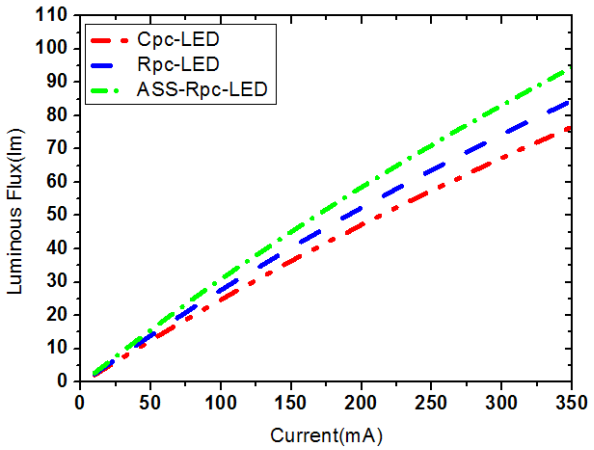

(a)

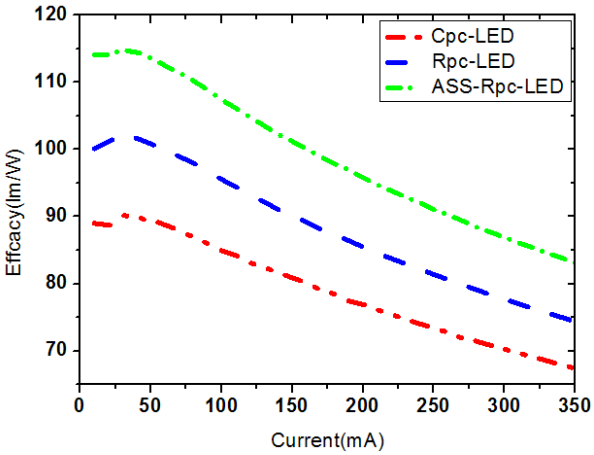

(b)

Fig. 8. (a) Variations in output luminous flux and (b) luminous efficiency as the function of injection current for the test LEDs

Comparing the results of Rpc-LED and ASS-Rpc-LED, we can see that the LEE have very obvious increasement when the ASS exist on the surface. In the spectral ranges of 400–700 nm, the LEE of the replicated prototype are about 11.76%, respectively. From simulation results in Fig. 3, the light extraction efficiency of a PET film with ASS having an interval of 350 nm and a height of 300 nm increased by approximately 13.30% than that without ASS. If we ignore the light loss during a PET film with ASS combined with Rpc-LED through UV curing process, we can set this value as the simulation

result of improvement in the light extraction efficiency of ASS-Rpc-LED. The difference between experiment and simulation results are 1.54%. It is seen that the difference is very small. That is, the experimental results are highly consistent with the simulation results in 400–700 nm range.

From the Fresnel reflection equation [23], the reflectance for s-polarized light is

$$R_s = \left(\frac{n_1 cos\theta_i - n_2 cos\theta_t}{n_1 cos\theta_i + n_2 cos\theta_t}\right)^2 \quad (2)$$

while the reflectance for p-polarized light is

$$R_p = \left(\frac{n_1 cos\theta_t - n_2 cos\theta_i}{n_1 cos\theta_t + n_2 cos\theta_i}\right)^2 \quad (3)$$

where n_1 and n_2 are the refractive indices of media 1 and 2, the angles that the incident and refracted rays make to the normal of the interface are given as θ_i and θ_t, respectively. We can predict when the rays pass through media with various refractive indices. The greater the difference in between the refractive indices of the two media is, the more apparent Fresnel reflections are in the rays. ASS can generate effects similar to the refractive index gradient. These structures form optical thin films with equivalent refractive indices, which reduce the difference in the refractive indices between the two media. It can suppress Fresnel reflections substantially for rays with a wider range of wavelengths and incident angles [24, 25]. Since the luminous efficiency of the Cpc-LED is limited, due to scattering centers [26]. It is proved that the interface Fresnel reflection is reduced when the ASS film exists. The luminous efficiencies linearly the large difference in refractive index at the interface between the encapsulation layer and the air, the ASS film behaves as photon wave-guides and decrease with an increasing input current when the input current is over 30 mA. This is because of Nitride-based LEDs suffer from a droop of the internal quantum efficiency with increasing input current. This luminous efficiency droop phenomenon is observed across a broad wavelength spectrum of InGaN/GaN LEDs [27-29].

The optical properties of color coordinates, color temperature, and color rendering for three Rpc-LED samples produced using the same process are listed in Table 1. Moreover, the ASS PET films integrated on three Rpc-LED samples were measured. The results of the optical properties were almost the same as those without the ASS PET film; that is, the effect of the ASS film on the optical properties of color coordinates, color temperature, and color rendering was minimal and can be ignored.

Table 1. Optical properties of color coordinates, color temperature, and color rendering for three Rpc-LEDs

Sample	Color coordinate (x, y)	CCT (K)	CRI
1	(0.313, 0.310)	6879	73
2	(0.303, 0.330)	6953	76
3	(0.310, 0.311)	6853	75

5. Conclusions

In this study, the LEE of a remote phosphor white LED was enhanced using a hemiellipsoidal ASS PET film, which was fabricated to reduce the Fresnel reflection of the LED package surface. The completed ASS PET film was integrated on the Rpc-LED surface through a UV-curing adhesive process. The measured results show that the luminous efficiency was enhanced by approximately 11.76% when the ASS film was used. The luminous efficiency of the ASS-Rpc-LED is more than approximately 23.26% compared with that of the pc-LED. Moreover, the optical properties of color coordinates, color temperature, and color rendering of remote phosphor LEDs were not affected when the ASS film was present. The ASS PET film can enhance the luminous efficiency of Rpc-LEDs and does not affect their color characteristics.

References

[1] C. Sun, Y. Zhang, Y. Wang, W. Liu, S. Kalytchuk, S. V. Kershaw, T. Zhang, X. Zhang, J. Zhao, W. W. Yu, A. L. Rogach, Appl. Phys. Lett. **104**(26), 261106 (2014).
[2] J. K. Kim, H. Luo, E. F. Schubert, J. Cho, C. Sone, Y. Park, Jpn. J. Appl. Phys. **44**(21), 649 (2005).
[3] Y. Yang, Y. Ren, Y. Chen, M. Liu, W. Chen, X. Han, X. Lin, Q. Liao, W. Zang, H. Luo, J. Lin, Z. Wu, Y. Liu, B. Zhang, Microelectron. Eng. **139**, 39 (2015).
[4] C. Geng, L. Zheng, H. Fang, Q. Yan, T. Wei, Z. Hao, X. Wang, D. Shen, Nanotechnology **24**(33), 335301 (2013).
[5] P. Dong, J. Yan, J. Wang, Y. Zhang, C. Geng, T. Wei, P. Cong, Y. Zhang, J. Zeng, Y. Tian, L. Sun, Q. Yan, J. Li, S. Fan, Z. Qin, Appl. Phys. Lett. **102**(24), 241113 (2013).
[6] N. Okada, K. Tadatomo, Semicond. Sci. Technol. **27**(2), 024003 (2012).
[7] Y. Zhang, T. Wei, Z. Xiong, L. Shang, Y. Tian, Y. Zhao, P. Zhou, J. Wang, J. Li, Appl. Phys. Lett. **105**(1), 013108 (2014).
[8] T. I. Kuznetsova, N. A. Raspopov, Quantum Electronics **45**(11), 1055 (2015).
[9] H. W. Liu, Q. Kan, C. X. Wang, H. Y. Hu, X. S. Xu, H. D. Chen, Chin. Phys. Lett. **28**(5), 054216 (2011).
[10] H. Q. Li, C. Y. Miao, E. B. Li, Z. H. Liu, K. J. Wei, Laser Phys. Lett. **9**(12), 844 (2012).
[11] H. Luo, J. K. Kim, Y. A. Xi, E. F. Schubert, J. Cho, C. Sone, Y. Park, Appl. Phys. Lett. **89**(4), 041125 (2006).
[12] H. Luo, J. K. Kim, E. F. Schubert, J. Cho, C. Sone, Y. Park, Appl. Phys. Lett. **86**(24), 243505 (2005).
[13] X. X. Su, T. X. Ma, Y. S. Wang, C. Zhang, Phys. Scr. **86**(4), 045401 (2012).
[14] Y. S. Duksh, B. K. Kaushik, R. P. Agarwal, J. Semicond. **36**(5), 055002-1 (2015).
[15] M. Hagedon, J. Heikenfeld, J. Micromech. Microeng. **23**(11), 117005 (2013).
[16] Y. Deng, P. Yi, L. Peng, X. Lai, Z. Lin, J. Micromech.

Microeng. **24**(4), 045023 (2014).
[17] L. Peng, Y. Deng, P. Yi, X. Lai, J. Micromech. Microeng. **24**(1), 013001 (2014).
[18] H. F. Yang, H. D. He, E. L. Zhao, J. Han, J. B. Hao, J. G. Qian, W. Tang, H. Zhu, Laser Phys. **24**(6), 065901 (2014).
[19] E. C. Chang, D. Mikolas, P. T. Lin, T. Schenk, C. L. Wu, C. K. Sung, C. C. Fu, Nanotechnology **24**(45), 455301 (2013).
[20] T. W. Lin, C. F. Chen, J. J. Yang, Y. S. Liao, J. Micromech. Microeng. **18**(9), 095029 (2008).
[21] J. Escarré, C. Battaglia, K. Söderström, C. Pahud, R. Biron, O. Cubero, F. J. Haug, C. Ballif, J. Opt. **14**(2), 024009 (2012).
[22] E. Lausecker, M. Grydlik, M. Brehm, I. Bergmair, M. Mühlberger, T. Fromherz, G. Bauer, Nanotechnology **23**(16), 165302 (2012).
[23] E. Hecht, Optics, 4th ed., Addison Wesley (2002).
[24] C. W. Hsu, Y. C. Lee, H. L. Chen, Y. F. Chou, Photonics Nanostruct. **10**(4), 523 (2012).
[25] C. H. Sun, P. Jiang, B. Jiang, Appl. Phys. Lett. **92**(6), 061112 (2008).
[26] S. H. Kim, H. H. Park, Y. H. Song, H. J. Park, J. B. Kim, S. R. Jeon, H. Jeong, M. S. Jeong, G. M. Yang, Opt. Express. **21**(6), 7125 (2013).
[27] J. Piprek, Physica Status Solidi A Appl. Res. **207**(10), 2217 (2010).
[28] M. H. Crawford, IEEE J. Select. Topics Quantum Electron. **15**(4), 1028 (2009).
[29] H. Y. Ryu, D. S. Shin, J. I. Shim, Appl. Phys. Lett. **100**(13), 131109 (2012).

*Corresponding author: ccf@cc.ncu.edu.tw